Elutriation and Species Segregation Characteristics of Polydisperse Mixtures of Group B Particles in a dilute CFB Riser

Jia Wei Chew, Drew M. Parker, and Christine M. Hrenya
Dept. of Chemical and Biological Engineering, University of Colorado at Boulder, Boulder, CO 80309

DOI 10.1002/aic.13784
Published online March 19, 2012 in Wiley Online Library (wileyonlinelibrary.com).

Experiments in a dilute, gas-solids circulating fluidized bed have been conducted, with an emphasis on the impact of polydispersity on elutriation and species segregation. Two categories of polydispersity were studied: binary mixtures with various compositions and continuous particle size distributions (PSDs) with various widths. Qualitative differences between the two include (i) total elutriation flux of binary mixtures increases with the composition of fines ($U_t < U_s$) but not so for continuous PSDs and (ii) elutriation flux of coarse particles ($U_t > U_s$) depends non-monotonically on fines composition for binary mixtures but monotonically for continuous PSDs. These differences are explained by the increasing size disparity of continuous PSDs as distribution width increases, while the size disparity remains constant in binary mixtures of varying compositions. A third qualitative difference is the monotonic decrease in mass % of coarse particles with riser height observed for continuous PSDs, and a nonmonotonic behavior for binary mixtures. © 2012 American Institute of Chemical Engineers *AIChE J,* 59: 84–95, 2013

Keywords: binary mixture, continuous particle size distribution, Geldart Group B, circulating fluidized bed riser, elutriation, entrainment, species segregation

Introduction

Gas-solids circulating fluidized beds (CFBs) represent an important unit operation in industry, with applications spanning energy production (e.g., coal gasification), chemical synthesis (e.g., olefin polymerizationand titanium dioxide production), and pharmaceutical (e.g., granulation) processes. Moreover, polydispersity is prevalent in flows involving solids, and the presence of a range of particle sizes and/or densities is known to exert a critical influence on the performance of such operations. However, due to a lack of understanding of the impact of polydispersity on flow phenomena[1–4] (such as elutriation and species segregation), design and troubleshooting of such processes is often based on empirical correlations, resulting in erratic performance and adverse flow behavior.

The focus of this experimental effort is on polydisperse Geldart[5] Group B particles in a dilute CFB riser. In such a system, the elutriation and species segregation characteristics can significantly affect the performance of the system in terms of gas-solids contact, solids residence time, and heat and mass transfer. Accordingly, a suite of experiments has been performed aiming at understanding the impact of riser flow characteristics on Group B particles. Specifically, two categories of polydispersity are examined: (i) "binary" mixtures (two species with particle size (d_{ave}) and particle density (ρ_s) differences) and (ii) "continuous" particle size distributions (PSDs). More explicitly, the objectives of this work are to investigate the impact of varying the (i) compositions of binary mixtures and (ii) widths of continuous PSDs on the total and species elutriation flux, as well as local measurements of mass flux and species segregation.

With regards to the impact of polydispersity on elutriation flux, despite the abundance of elutriation correlations made available in the past few decades,[6–11] the discrepancy between empirical prediction and actual data reaches a hundred fold in some cases.[11] Hence, more understanding is warranted. It is well-established that at a fixed superficial gas velocity (U_s), overall elutriation flux is negatively correlated with the single-particle terminal velocity (U_t) for a monodisperse system, and directly proportional to composition of elutriable species in a polydisperse mixture.[6–11] Accordingly, if the composition of fine species (i.e., particles with $U_t < U_s$) increases, total elutriation flux is expected to increase linearly, and vice versa. However, exceptions to the correlations have been noted in the literature. For example, for binary mixtures, it has been reported that the elutriation flux increases with the composition of the fine species (which belong to Geldart Group A or C) if that species is above a critical size,[12–14] otherwise the elutriation flux plateaus or even decreases due to the dominance of interparticle cohesion.[12–14] Of particular interest in this work is the counter-intuitive elutriation behavior of the coarse species (i.e., particles with $U_t > U_s$) in a binary mixture reported by Geldart et al.[15] More specifically, it was found the presence of Group A fine species in the binary mixture boosts the

Correspondence concerning this article should be addressed to C. M. Hrenya at hrenya@colorado.edu.

elutriation flux of the coarse particles to higher than that of monodisperse coarse particles (i.e., 100% coarse), and also the elutriation flux of the coarse exhibits a nonmonotonic behavior (increasing and then decreasing) with respect to the fine composition.[15] To date, no information is available on how binary mixtures of Group B particles with varying compositions affect elutriation. Perhaps more importantly, previous work on how the width of continuous PSDs affects elutriation has not been reported. Hence, finding an answer for the two corresponding questions are attempted in this work. First, since the fine species previously reported belongs to Group A,[15] and bearing in mind the differences between Groups A and B particularly in terms of fluidization behavior[5] and Stokes number,[16] will the counter-intuitive (nonmonotonic) behavior of the coarse persist if the fine species in the binary mixture belongs to Group B? Second, noting the qualitatively different behaviors between binary mixtures and continuous PSDs previously reported for bubbling beds[17,18] and CFBs,[19–21] how does the elutriation flux of coarse particles behave for continuous PSDs with changing distribution widths?

Pertaining to species segregation, both experiments and simulations have indicated that particles segregate according to species in both granular systems[22–28] (absence of gas phase) and fluidized systems.[4,8,29–38] However, although investigation into species segregation behavior in low-velocity bubbling fluidized beds has been fairly extensive (refer to Refs. [8,29,39–41] and references cited therein), a similar effort for CFBs is more limited. With regards to axial segregation, both experiments[19,30–32,42–45] and simulations[33,37,44,46] have revealed that the more massive species segregates toward the bottom of the riser. As for radial segregation, both simulation results[33,36,38] and experimental data[19,31,32,44,45] consistently indicate that the more massive species preferentially segregate toward the wall. The physical explanation for the radial segregation is related to the expected radial granular temperature gradients in a riser.[33,46–51] Specifically, the more massive species have a tendency to segregate preferentially toward the lower temperature region due to thermal diffusion.[4,33] Concomitantly, it has been shown via both experiments[49,50] and kinetic-theory-based models[33,36,47,48,51] that lower granular temperature regions are found at the wall due to augmented dissipation of kinetic energy through particle-wall collisions and increased particle–particle collisions due to the higher solid volume fraction expected in the annular region (i.e., core-annulus flow). A logical ensuing question arises: if the radial granular temperature gradient and hence radial segregation is due in part to core-annular riser flow, does radial segregation still persist in a dilute riser where the core-annulus behavior is reduced? Another question is motivated by previous work that indicates binary mixtures and continuous PSDs display different species segregation trends in bubbling fluidized beds[17,18,52–54] as well as higher-velocity, denser risers.[19] In particular, do binary mixtures and continuous PSDs also exhibit different segregation patterns in a dilute riser?

With the above questions in mind, the current work is divided into two categories of polydisperse, dilute risers: binary mixtures (two species with different particle size, d_{ave}, and material density, ρ_s) and continuous PSDs. The objectives of this work are to experimentally investigate the impact of changing the compositions of binary mixtures and widths of continuous PSDs on total and species elutriation flux, as well as local mass flux and species segregation. The results indicate that the binary mixtures and continuous PSDs display different trends for (i) the total elutriation flux versus the composition of fine particles ($U_t < U_s$), (ii) the dependency of the elutriation flux of the coarse species ($U_t > U_s$) on the composition of fine particles, and (iii) the axial species segregation at the wall. Other insights obtained include the link between coarse elutriation and collisional transfer mechanism, the flattening of radial mass flux profiles as fine composition increases for binary mixtures or width (σ/d_{sm}) increases for continuous PSDs, and the lack of significant radial segregation, presumably due to the flatter radial granular temperature gradients that exist in the dilute riser.

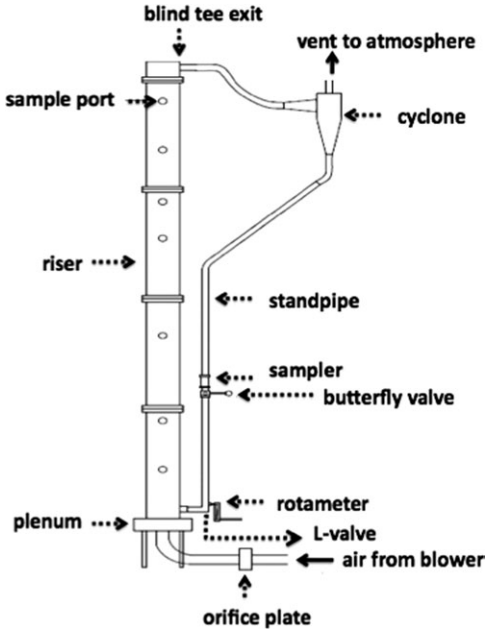

Figure 1. Experimental set-up.

Experimental Methods

Experimental apparatus

All experiments were performed in a CFB, schematically shown in Figure 1. The riser section is a Plexiglas column which is 18.4 cm in diameter and 4 m tall, with a blind-tee exit at the top. A cyclone after the riser exit enables recirculation of the solids, and solids are fed back to the riser through an aerated *L*-valve. A Yaskawa V7 variable frequency drive, which is controlled by a National Instruments LabVIEW program (version 7.1), directs a Fuji Electric VFD5 regenerative blower that provides the air for fluidization of the particles. The superficial gas velocity (U_s), which is reported at local atmospheric conditions (air with a 0.97 kg/m^3 density and 1.85×10^{-5} Pa s viscosity), is determined via a Lambda Square Oripac 4150-P orifice plate flow meter, which is located upstream of the plenum. Relative humidity (RH) in the unit is enhanced by an Air-O-Swiss model AOS 7144 humidifier placed at the inlet of the blower. RH is kept above 40% for all experiments to reduce electrostatics.[55–58] The operating air temperature and RH in the plenum are measured by means of an Omega HX93AV-RP1 probe, with a temperature range from −4 to 171°C and RH range of 0–100%, inserted into the plenum. The distributor at the bottom of the riser is a Mott Corporation 316 stainless steel sintered porous plate, of Media Grade 100 and thickness of

Table 1. Experimental Parameters for Binary Mixtures

Material	Glass	PS
ρ_s (kg/m^3)	2500	1050
d_{ave} (μm)	165	327.5
U_t (m/s)[60]	1.2	1.6
Mass (%)	0, 25, 50, 75, 100	100, 75, 50, 25, 0
U_s (m/s)	1.5	1.5

2.4 mm. The pressure drops across the orifice plate flow meter, across the distributor plate, and along the entire riser are measured using Orange Research 20100 Series low-differential pressure transmitters with the ±0.2% accuracy option. Pressure drop statistics across the orifice meters are transmitted to the computer and superficial velocities are computed. All temperature, RH, superficial velocity, and pressure data are recorded throughout the experiments.

Sample ports are available approximately equally spaced along the riser height for insertion of the extraction probe, which is used for measurement of local mass flux and species segregation characteristics. Up to three sample ports each 90° azimuthally apart on the horizontal plane are available at each of these axial positions to detect potential flow asymmetries. A sampler device in the standpipe allows for measurement of the total elutriation flux (mass flux of particles carried out of the top of the riser). Specifically, a butterfly valve at the bottom of the sampler was closed at the same instant that a stopwatch was started. When the sampler filled up, the CFB was shut down and the stopwatch was stopped. Then, the sampler was removed, and the particles were collected and weighed. A total elutriation flux was hence obtained through dividing the mass of particles in the sampler by the product of the cross-sectional area of the riser and the duration of collection.

Materials investigated and operating conditions

As summarized in Tables 1 and 2, the materials studied here are binary mixtures (Table 1) and continuous size distributions (Table 2) of Geldart Group B particles. For the binary mixtures, various compositions of the two species, namely glass and polystyrene (PS), which differ in both (mass-based) average particle diameter (d_{ave}) and material density (ρ_s), were examined. For the continuous PSDs, various PSD widths were examined using sand. The single-particle terminal velocity (U_t) of each species and the superficial gas velocity (U_s) used for the two mixture types (i.e., binary mixture and continuous PSD) are also listed in the tables. Specifically, the U_t of each material and the implemented U_s are important considerations, because in an ideal scenario with a single particle in infinite fluid, the particle can be elutriated (carried over) only if U_s exceeds U_t. Correspondingly, many correlations for estimating elutriation rate are based on either $U_s - U_t$ or U_s/U_t.[6–11] For all experiments, several parameters were kept constant for direct comparison among the mixtures, namely (i) CFB inventory (8 kg of particles) since bed depth and elutriation rate are correlated,[59] and (ii) U_s within each of the two sets (i.e., binary mixtures and continuous PSDs) of experiments since the driving force for elutriation is linked to $U_s - U_t$ or U_s/U_t.[6–11] Conversely, the parameters varied are compositions of the binary mixtures and the widths (defined as ratio of standard deviation of the PSD to Sauter-mean diameter, σ/d_{sm}) of the continuous PSDs. Accordingly, five different binary mixtures (mass % of glass = 0, 25, 50, 75, and 100%) and five different continuous PSDs (σ/d_{sm} = 5, 10, 25, 40, and 65%, with d_{sm} held constant) were investigated. Finally, a dilute riser is the focus of this work, with solid loadings (m, which is the ratio of solid flux to air flux) in the ranges of 0.03–0.25 for the binary mixtures and 0.11–0.29 for the continuous PSDs.

With regards to the binary mixtures, glass and PS particles were mixed in various compositions, as listed in Table 1. Glass beads purchased from Grainger were sieved to obtain only sizes that fall between the 150 and 180 μm sieves, whereas PS beads purchased from of Glen Mills Incorporated were sieved to restrict sizes to those between the 300 and 355 μm sieves. Notably, the terminal velocity (U_t) of the glass beads is lower than the implemented U_s, and will be referred to here as "fine"[15]; whereas the U_t of PS is higher than U_s, and will be referred to here as "coarse."[15] Accordingly, the binary mixtures investigated encompass the entire range of compositions, including (i) monodisperse coarse (i.e., 100 mass % coarse), (ii) 75 mass % coarse (and 25 mass% fine), (iii) 50 mass % coarse, (iv) 25 mass % coarse, and (v) monodisperse fine (i.e., 100 mass% fine). Ideally (for a single particle in infinite fluid), particles with $U_t < U_s$ should be elutriated (i.e., performed on the top of the riser), whereas particles with $U_t > U_s$ should not. However, this cutoff is not strictly appropriate in the CFB riser since presence of surrounding particles impacts the settling velocity, and the concept of the "hindered settling velocity"[10,61] (i.e., the settling velocity of a particle in suspension, which is known to be lower than that of an isolated particle) is thus more relevant. Accordingly, the value of U_s used in the experiments was chosen to be high enough to enable elutriation of the monodisperse coarse particles and low enough to restrict the total elutriation flux of the monodisperse fine particles to a practical level. With regards to the latter, when the total elutriation is too high, the cyclone is inefficient in returning solids to the recirculation loop, and the sampler fills up too fast to enable an accurate measurement using the stopwatch. It was found experimentally that U_s = 1.5 m/s was optimal, since it allowed for measureable elutriation of just coarse particles (one monodisperse limit of binary mixture composition) on one hand, while also restricting the level of elutriation of just fine particles (other monodisperse limit of binary composition) to reasonable levels on the other.

As for the continuous PSDs (Table 2), Gaussian and log-normal distributions were made up of sand particles with a wide range of particle sizes largely within the Geldart Group B classification.[5] The equation defining the mass-based frequency distribution (f_m) of Gaussian distributions is

$$f_{m,Gaussian}(x) = \frac{1}{\sigma\sqrt{2\pi}} \exp\left[-\frac{(x-\bar{x})^2}{2\sigma^2}\right] \quad (1)$$

Table 2. Experimental Parameters for Continuous PSD

Material	Sand
ρ_s (kg/m^3)	2650
d_{sm} (μm)	196
$U_{t,dsm}$ (m/s)[60]	1.6
Range of d_{ave} (μm)	79.5–780
Range of U_t (m/s)	0.40–6.5
σ/d_{sm} (%)	5, 10, 25, 40, 65
U_s (m/s)	1.7

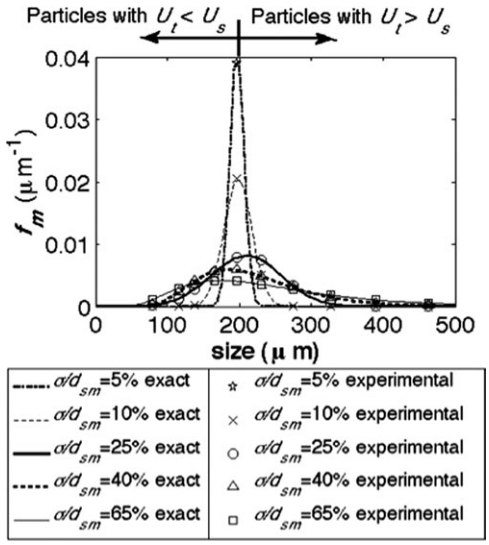

Figure 2. PSDs of lognormal distributions investigated, with d_{sm} kept constant at 196 μm and σ/d_{sm} varied.

The lines represent exact mass-based lognormal distributions as defined by Eq. 2, while the discrete points are experimental values.

where σ is the standard deviation of the mass-based PSD, x is particle diameter, and $\bar{x}$ is the arithmetic mean of the mass-based PSD. Analogously, the mass-based lognormal distribution is defined as

$$f_{\mathrm{m,lognormal}}(x) = \frac{1}{x\sigma_\mu\sqrt{2\pi}}\exp\left[-\frac{(\ln(x)-\mu)^2}{2\sigma_\mu^2}\right] \qquad (2)$$

whereby the natural logarithm of this distribution is a Gaussian PSD with arithmetic mean μ and standard deviation σ_μ. In this work, d_{sm} is kept constant and the widths of the continuous PSDs (denoted σ/d_{sm}) are varied. The d_{sm} is used instead of other characteristic diameters since it is the most physically relevant. Namely, d_{sm} is the ratio of the volume-based to surface-based diameters, the former of which is proportional to the gravitational force and the latter of which is proportional to the drag force. Correspondingly, to compute the Sauter-mean diameter (d_{sm}),[10] the mass-based distributions (f_m) in Eqs 1 and 2 are converted to the corresponding number-based PSDs (f_n), and then d_{sm} is determined as $\frac{\int x^3 f_n}{\int x^2 f_n}$.

Accordingly, the narrowest distribution possible is $\sigma/d_{sm} = 5\%$, in which all particles fall within one sieve cut (180–212 μm), as shown in Figure 2. Conversely, the widest distribution examined is $\sigma/d_{sm} = 65\%$, above which would require a considerable amount of Group A particles (<100 μm), which is avoided since the focus here is on Group B materials. Furthermore, since Gaussian distributions (Eq. 1) are restricted to $\sigma/d_{sm} < 30\%$ (greater values of σ/d_{sm} involve unphysical negative diameters[62]), lognormal distributions are used for the wider PSDs investigated. Notably, because Gaussian and lognormal distributions are similar in shape for $\sigma/d_{sm} < 30\%$,[25] the three narrowest distributions investigated (namely, $\sigma/d_{sm} = 5$, 10, and 25%) can be referred to as either Gaussian or lognormal, but will be referred to as lognormal from here onward.

To prepare the continuous PSDs, sand acquired from Agsco Corporation was classified into different sizes using various Fisher brand US standard brass sieves. Figure 2 shows the exact lognormal distributions (Eq. 2) as solid lines and corresponding sieve fractions used in the experiments as discrete points. For the experiments, f_m refers to the mass fraction of each sieve cut normalized with respect to the bin width (i.e., Δx) of a given sieve cut. The choice of d_{sm} is such that it has to be high enough such that particles still largely belong to Geldart Group B even for the widest PSD (Figure 2), while low enough such that the corresponding single-particle terminal velocity (U_t) is less than the maximum limit of superficial air velocity ($U_{s,max}$) that the blower can generate to ensure elutriation. Accordingly, since $U_{s,max}$ is 1.7 m/s, the largest sand particle that can be ideally elutriated is of 202 μm. Because of the restriction of sieve sizes available, however, the d_{sm} was set to 196 μm, which is the average size between two sieve cuts (180 and 212 μm) and has a U_t of 1.6 m/s (Table 2). Subsequently, the value of $U_s = 1.7$ m/s was used for all the continuous PSDs investigated. Finally, it is noted that sand attrits over time, and hence to preserve the integrity of the PSD, a fresh PSD was prepared after every three cumulative hours of experimental runs, since preliminary checks on 8 kg of particles which fall between the 180 and 212 μm sieves showed that only 85 mass % (i.e., greater than acceptable tolerance of 10 mass %) of the bed retained the original size range at the end of 3 h.

Measurement technique

To characterize local mass flux and species segregation in the riser, an extraction probe fabricated by Particulate Solid Research Incorporated was used to collect particles at various axial and radial positions along the riser, after which the PSD of each sample was analyzed using sieves. The extraction probe has an inner diameter of 0.011 m, with the probe tip oriented at 90° to the probe shaft to collect particles in the direction of mean flow in the riser. It is worth noting that the extraction probe was operated non-isokinetically[63–67] (i.e., the suction velocity obtained via the vacuum pump is not necessarily identical to the solids velocity), after checks were made to ensure that the measurements were not dependent on suction velocity. The successful implementation of non-isokinetic operation on Group B particles is not surprising, since the associated higher Stokes number of the more massive particles implies that the particles are less adept at following the gas streamlines. For the PSD analysis, one sieve sized at 212 μm was used to separate the constituents of the binary mixtures, whereas seven sieves in the size range of 53–300 μm were used for the continuous PSDs.

Samples were collected at five approximately equally spaced axial positions along the riser, with the lowest axial position at a dimensionless height (h/H, where h is the axial position where measurement was taken and H is the total riser height) of 0.43. At each axial location, two sets of six radial measurements (from riser center to opposite wall) that are 90° apart in the horizontal plane were taken to determine if any asymmetries were present across the riser cross-section. Notably, due to the curvature of the probe, the three radial positions closest to the insertion port could not be measured, hence only the radial portion from the wall opposite to the insertion port to the riser center was characterized. Using the extraction probe, both the upward and downward mass flux at each local radial position (G_r) was measured by orientating the probe tip normal to the flow in the associated

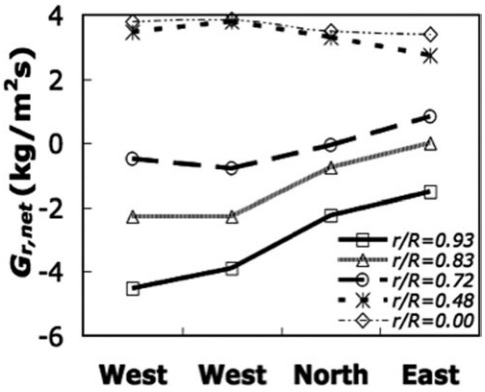

Figure 3. Variation of flux at wall for lognormal PSD with σ/d_{sm} = 40% at h/H = 0.43, when probe is traversed in different azimuthal directions 90 degrees apart on the horizontal plane, namely, toward the West, North, and East directions.

direction. At each location, particles were collected for 20–40 s. The net mass flux (i.e., total elutriation flux) across the cross-section of the riser at a given axial position is denoted G_s and calculated as follows

$$G_s = \sum_{r=1}^{\substack{11\text{radial}\\ \text{positions}}} [(G_{r,upward} - G_{r,downward}) \times A_r] \quad (3)$$

where G_r refers to local flux at radial position r, the subscripts upward and downward refer to the flux directions and A_r is the annular area corresponding to that radial position. For example, for radial position r_j, the corresponding annular area has an outer and inner radius of $(r_j + r_{j+1})/2$ and $(r_j + r_{j-1})/2$, respectively. Notably, G_s can be measured two ways: (i) integration of the local flux measured by the extraction probe using Eq. 3, and (ii) direct measurement using the sampler in the standpipe of the CFB (Figure 1). Using the two methods provided validation for the total elutriation flux, as described below.

To further validate the extraction probe measurements, checks were made with regards to (i) reproducibility of mass flux measurements between repeated runs, and (ii) consistency of the local mass flux integrated across the riser cross-section at each axial position, which ensures a mass balance. Accordingly, Figure 3 is a plot of local flux ($G_{r,net} = G_{r,upward} - G_{r,downward}$) measured at $h/H = 0.43$ at various radial positions when the probe was traversed in different azimuthal directions, namely, toward the West (two repeated runs), North and East directions. Measurement toward the South was not possible because the standpipe obstructs probe insertion. For (i), agreement was obtained within an acceptable tolerance of 10%, as depicted in Figure 3, whereby repeated West measurements agree well at each radial location. With respect to (ii), as shown in Figure 3 and corroborating with previous work,[64,67] considerable variations are observed near the wall ($r/R = 0.93$) at different azimuthal locations, with such variations decreasing toward the riser center ($r/R = 0$). Accordingly, the local wall flux was averaged over different azimuthal directions to calculate the integrated mass flux (Eq. 3), which agreed well with that measured directly in the standpipe (within ±10%). In addition, since species segregation is a focus of this work, it is important to check if the PSDs at the wall vary with the different values of $G_{r,net}$ at different azimuthal positions. As seen in Figure 4, the overall PSDs (i.e., PSDs from both upward and downward fluxes are accounted for, with the flux from each direction weighted according to contribution to the net flux) at different azimuthal positions near the wall are similar despite the azimuthal differences in local $G_{r,net}$ (Figure 3).

Finally, to express a representative mass flux at each radial position, a net mass flux normalized with respect to G_s at the same axial position is defined as

$$G_{r,net,norm} = \frac{G_{r,upward} - G_{r,downward}}{G_s} \quad (4)$$

Because of the experimental variations of approximately 10% in G_s at each axial position, this normalization is performed to present fairer comparisons between the different axial locations. Moreover, the normalization is helpful for a straightforward comparison among the various binary mixtures and continuous PSDs, since the total elutriated flux (G_s) varies from mixture to mixture.

Results and Discussion

A key qualitative difference between binary mixtures and continuous PSDs is that while the former involves two fixed species (with differences in particle size, d_{ave}, and material density, ρ_s) at varying compositions, the continuous PSD's have particles with fixed ρ_s but an increasing range of particle diameters (i.e., more species) as σ/d_{sm} increases. In particular, referring to Figure 2, increasing σ/d_{sm} for continuous PSDs increases the range of both fine and coarse particle sizes. For this reason, the two mixture types are covered separately below. Quantities of interest include the elutriation flux of particles from the riser (total and species), the local profiles of both mass flux and species segregation.

Binary mixtures

For the set of experiments involving binary mixtures, three plots are presented in Figure 5 as functions of mass % of fine: (a) total elutriation flux (G_s), (b) fine (glass) elutriation flux, and (c) coarse (PS) elutriation flux. The data points represent the average values of two repeat measurements, and the error bars represent the span of the repeats. Notably, the left-hand side of the x-axes refer to monodisperse coarse (i.e., 100 mass % of PS), and vice versa. It is shown in Figure 5a that as the mass % of fine in the system increases, the total elutriation flux increases approximately linearly.

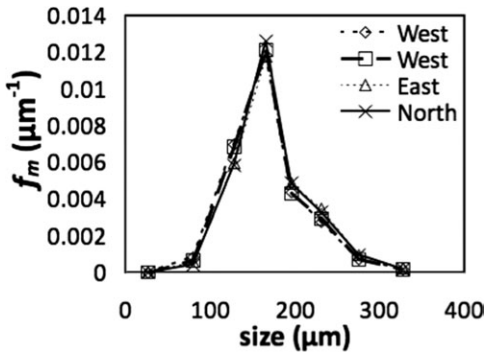

Figure 4. Reproducibility of total PSDs of lognormal PSD with σ/d_{sm} = 40% at h/H = 0.43 and r/R = 0.93 at different azimuthal locations.

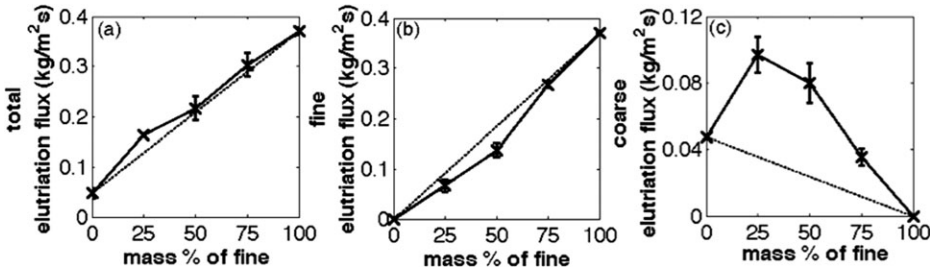

Figure 5. (a) Total elutriation flux (G_s), (b) fine elutriation flux, and (c) coarse elutriation flux of various compositions of binary mixtures investigated at U_s = 1.5 m/s.

Dotted lines represent simple linear relationship as per available correlations,[7,9,10] while solid lines connect experimental data points.

Recall from Table 1 that $U_{t,fine} < U_s$ and $U_{t,coarse} > U_s$. Accordingly, increasing the mass % of fine increases composition of the species with the smaller U_t, and hence the total elutriation rate increases. This trend is consistent with existing empirical correlations[7,9,10] which indicate that total elutriation flux is directly proportional to the composition of each fine species present in the system (as per Zenz and Weil,[68] $G_s = \sum_{\text{species}}^{\text{all elutriable}} x_i G^*_{s,i}$, where G_s is the total elutriation flux, x_i is the composition of elutriable species i, and $G^*_{s,i}$ is the elutriation flux from a bed consisting only of species i).

Figure 5b and c further show the variation of the species elutriation flux as the composition of fine in the system increases. It is observed that the elutriation of fine exhibits a monotonic increase (Figure 5b), whereas the elutriation of coarse exhibits a nonmonotonic trend (Figure 5c). In other words, whereas the elutriation of fine is lower in all binary mixtures compared to the monodisperse fine counterpart, the same is not true for the coarse species, since the elutriation of coarse is larger than its monodisperse counterpart at some compositions (mass % of fine $\leq$ 50%). Although this finding has not been reported for binary mixtures consisting of two Group B materials, Geldart et al.[15] made the same observation for a mixture of Groups A and B materials. This nonmonotonic behavior can be explained by the collisions occurring between fine and coarse particles. Specifically, the faster-moving fine particles ($U_t < U_s$) approach the coarse particles ($U_t > U_s$) and collide with them preferentially from the bottom, causing a net upward force on the coarse particles which allows the coarse to elutriate.[15] Two other physical explanations for the elutriation of the coarse are possible, but less likely. First, if the gas velocity profile is parabolic (or, more generally, nonuniform), the gas velocity in the riser core would be higher than U_s,[6,69] and thus the coarse may elutriate if located at the riser core. However, dilute flows as considered in this work are characterized by relatively flat (turbulent) gas velocity profiles.[69] Furthermore, particles are known to move laterally across the riser. Hence, the elutriation of coarse particles due to their location at a radial position characterized by a higher-than-average gas velocity is unlikely. The other possible explanation is linked to the concept of a "hindered settling velocity,"[10,61] in which the settling velocity of a particle in suspension is known to be lower than that of an isolated particle. However, based on the Einstein correction[10] for such effects, the hindered settling velocity for a particle in similarly dilute suspensions (void fraction ~0.999, based on other works with similar m)[70,71] is 99.6% of that of an isolated particle. Therefore, the collisional transfer mechanism described above is the most likely cause for the elutriation of coarse particles.

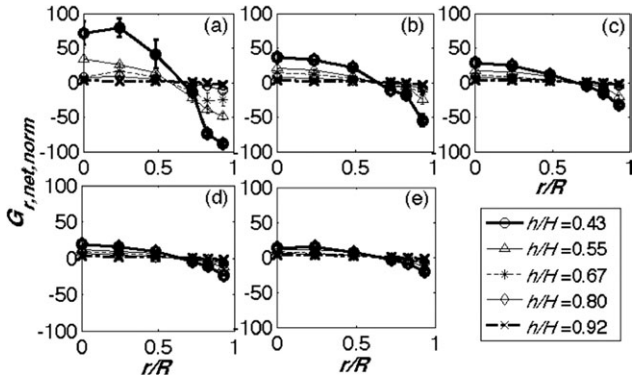

Figure 6. Radial $G_{r,net,norm}$ profiles for (a) monodisperse coarse, (b) 25 mass % fine, (c) 50 mass % fine (d) 75 mass% fine (e) monodisperse fine.

In particular, the collisional transfer mechanism explains the left-hand portion of Figure 5c in which the elutriation of coarse particles increases with the composition of fine particles in the system. Conversely, on the right-hand-side (mass % of fine >50%) of Figure 5c, the effect of the decreasing composition of coarse particles takes over. Namely, decreasing the mass % of coarse particles (increasing the fines content) reduces the maximum possible value of coarse elutriation until the zero limit is reached when only fine particles are present. Hence, the nonmonotonic elutriation of coarse particles stems from a trade-off in which an increased collisional momentum transfer from fine to coarse particles dominates at lower fine contents and a decreasing amount of coarse particles dominates at high fine content.

Now that the impact of composition on the elutriation (G_s) of particles from the riser has been established, it is worthwhile to examine the impact of composition on the radial (local) profiles of flux measurements (G_r). The normalized radial profiles of net flux ($G_{r,net,norm}$) are illustrated in Figure 6, with each subplot containing a graph of $G_{r,net,norm}$ (Eq. 4) versus r/R (where r is the radial position at which measurement was taken, and R is the riser radius). Each of the five subplots represents a different composition and contains five profiles measured at different axial positions. Consistent with previous work,[20,67,72–76] the radial profiles flatten with increased height. More interestingly, increasing the fine composition results in flatter radial $G_{r,net,norm}$ profiles at lower axial positions, which has not been previously reported.

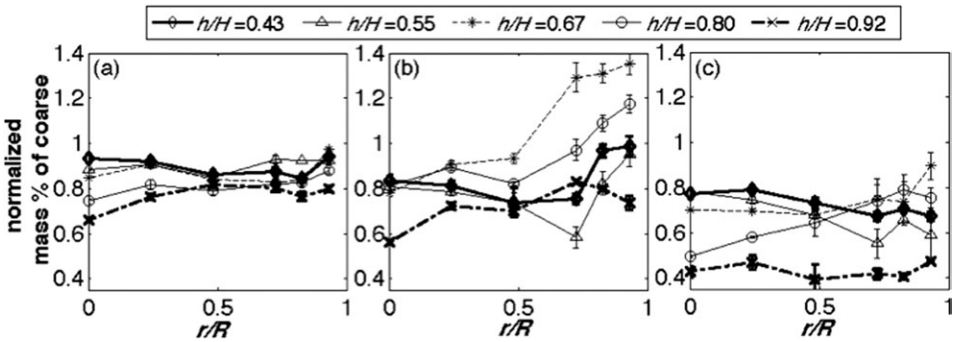

Figure 7. Radial segregation profiles of local mass % of coarse normalized with respect to the system mass % of coarse for binary mixtures with (a) 25, (b) 50, and (c) 75 mass % of fine.

Finally, the impact of the binary composition on species segregation is also of interest. Radial and axial species segregation profiles are displayed in Figures 7 and 8, respectively. These species (composition) segregation profiles are obtained by sieving the particles collected from the extraction probe at a given location. For a direct comparison of species segregation among the various mixture compositions, the measured mass fractions of coarse particles (PS) have been normalized with respect to the total mass fraction of coarse particles in the system, and are shown on the ordinate. Although Figure 7 depicts normalized mass % of coarse particles versus r/R (radial segregation), Figure 8 depicts h/H versus the normalized mass % of coarse (axial segregation). Each subplot in Figures 7 and 8 contains the various compositions (25, 50, and 75 mass % of fine) investigated, and the ranges of x- and y-axes are kept constant within each figure for a straightforward comparison.

Radial species segregation profiles are displayed in Figure 7, with each profile in a given plot representing the different riser axial positions where measurement was taken. It is observed that radial profiles are relatively flat at all axial positions for the three binary mixtures, except for a couple of profiles in the binary mixture with 50 mass % of fine (Figure 7b) which show a preferential segregation of the coarse particles toward the wall ($r/R = 1$). Notably, the radial segregation of the more massive species to the wall has been reported in previous simulation[33,36,38] and experimental[19,31,32,44,45] work on riser flow. Nonetheless, the generally negligible species segregation displayed in Figure 7 is not surprising since species segregation is linked to granular temperature gradients,[4,33,46–51] and the radial granular temperature profile is expected to be relatively flat (i.e., small gradient) in dilute systems.[71] Again, these flat profiles stem from the important role of turbulence in dilute systems relative to their denser counterparts.

Regarding species segregation in the axial direction (Figure 8), profiles at each radial position are given in each subplot. It is observed that, at $r/R = 0$, the mass % of coarse generally decreases with height, which agrees with previous work that indicated an overall (i.e., integrated across the cross-section) decrease of the more massive species with height.[19,30,31,45] Conversely, the mass % of coarse particles increases and then decreases with height near the wall ($r/R = 1$), corroborating with the results of Chew et al.[19] Similar to the radial segregation results (Figure 7), the binary mixture with 50 mass % of fine (Figure 8b) exhibits the greatest extent of axial segregation.

Continuous PSDs

Analogous to Figure 5 for binary mixtures, the total, fine and coarse elutriation fluxes for the continuous PSDs are shown in Figures 9a, c, respectively, as functions of PSD width (σ/d_{sm}). Comparing Figures 5 and 9, reveals a key difference between binary mixtures and continuous PSDs: while the coarse elutriation flux is nonmonotonic for binary mixtures (Figure 5c), it is monotonically decreasing for continuous PSDs (Figure 9c). As the quantity plotted on the x-axes of Figures 5 and 9 are not the same – composition of fine is plotted for binary mixtures (Figure 5) and the distribution width is plotted for the continuous PSDs (Figure 9) – it is worthwhile to investigate how the composition of fine particles changes with the width of the continuous PSD.

Based on the results displayed in Figure 9 for the continuous PSD and the explanation of trends discussed in conjunction

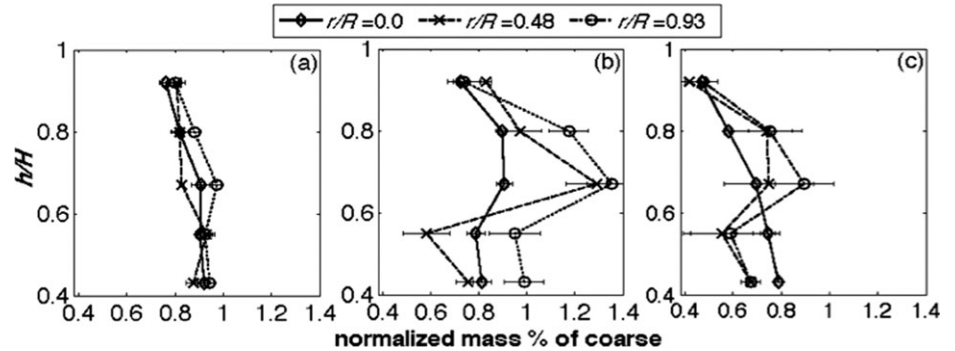

Figure 8. Axial segregation profiles of local mass % of coarse normalized with respect to the total system mass % of coarse for binary mixtures with (a) 25, (b) 50, and (c) 75 mass % of fine.

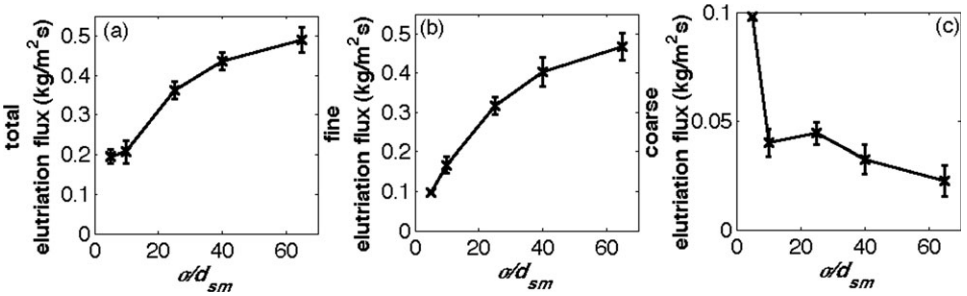

Figure 9. (a) Total elutriation flux (G_s), (b) fine elutriation flux, and (c) coarse elutriation flux of continuous PSDs as functions of σ/d_{sm} investigated at U_s = 1.7 m/s.

with Figure 5 for the binary mixtures, it is tempting to deduce that the fine content in continuous PSDs increases with distribution width (σ/d_{sm}). Put another way, if the elutriation of fines is proportional to their composition (consistent with composition-based elutriation correlations[7,9,10] and the observed behavior for binary mixtures – see Figure 5b) and if the fines content increases with σ/d_{sm} for continuous PSDs, the trends in Figures 9a, c are consistent with this physical picture. However, Figure 10a shows just the opposite, as σ/d_{sm} increases, the mass % of fine in the system actually decreases. Accordingly, continuous PSDs behave in stark contrast to binary systems since the elutriation of fine particles for continuous PSDs is not proportional to their composition in the system.

To sort out this inconsistency, a consideration of both the system (initial) PSD and the elutriated (entrained out of riser) PSD for the continuous distribution is warranted, as displayed in Figures 10 and 11, respectively. In each figure, the first row shows composition (mass %) of fine (particles with $U_t < U_s$) and coarse (particles with $U_t > U_s$) as functions of σ/d_{sm}. In the second row of each figure, the mass-averaged diameter of the fine (d_{fine}) and coarse (d_{coarse}) particles is also plotted versus σ/d_{sm}. A comparison of Figures 10 and 11 reveals a key difference – although the composition of fine decreases in the system PSD with an increase in σ/d_{sm}, the opposite is true of the elutriated PSD. The explanation for this difference lies in the second row of figures. As illustrated in Figure 10c, as the σ/d_{sm} of the initial (system) distribution increases, d_{fine} becomes smaller. Because smaller particles are easier to elutriate (recall U_s is held constant for all experiments and U_t decreases as particle size decreases), a larger percentage of the fine particles present in the system are performed on the top of the riser (elutriated). This increased percentage is sufficient to compensate for the reduced mass % of fine in the system as σ/d_{sm} increases (Figure 10a), leading to an increasing mass % of elutriated fines with σ/d_{sm} (Figure 11a). Similar arguments explain the trends observed for the coarse particles (subplots b and d in Figures 10 and 11). It is important to note that such arguments are not applicable to binary mixtures, since the average size of the fine and coarse particles remain constant, and only the composition of the two species changes.

It is now worthwhile to return to the first difference noted between the binary mixture and continuous PSD, namely the nonmonotonic elutriation of coarse particles in the former (Figure 5c) but not in the latter (Figure 9c). Recall the nonmonotonic behavior was explained via a trade off between the increased collisional momentum transfer to the coarse particles as the fine content increases and the corresponding decreased composition of the coarse particles. A possible explanation for the monotonic behavior of the continuous PSD may again be traced to the increased disparity in size of the fine and coarse particles (which is not the case for the binary mixtures). Namely, the collisional momentum transfer is proportional to particle mass, and thus collisional transfer becomes less effective as the size disparity (σ/d_{sm}) increases. In addition, the increasing mass-averaged diameter of the coarse particles (d_{coarse}) with σ/d_{sm} (Figure 11d) makes these particles harder to elutriate.

To now consider more local measurements, the radial mass flux profiles are shown in Figure 12 for each of the continuous PSDs. As expected, radial profiles flatten with riser height, which agrees with the binary results obtained here (Figure 6) and previous work on monodisperse and binary systems.[20,67,72–76] In addition, as σ/d_{sm} increases, radial

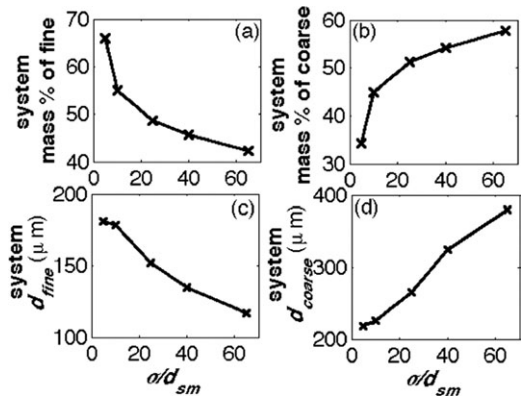

Figure 10. System PSD parameters as functions of σ/d_{sm}: (a) mass % of fine, (b) mass % of coarse, (c) d_{fine}, and (d) d_{coarse}.

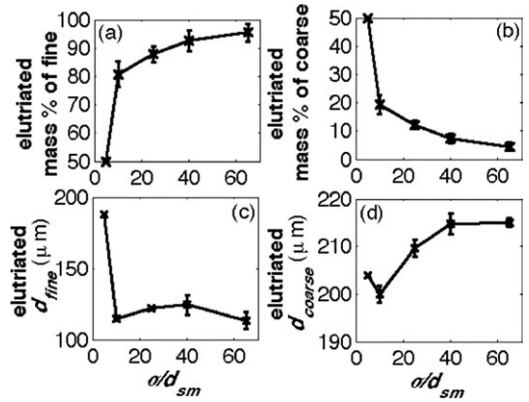

Figure 11. Elutriated PSD characteristics as functions of σ/d_{sm}: (a) mass % of fine, (b) mass % of coarse, (c) d_{fine}, and (d) d_{coarse}.

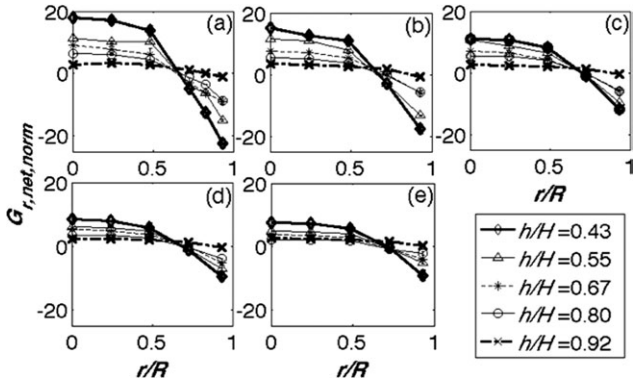

Figure 12. Radial $G_{r,net,norm}$ profiles for lognormal PSDs with σ/d_{sm} = (a) 5%, (b) 10%, (c) 25%, (d) 40%, and (e) 65%.

$G_{r,net,norm}$ profiles become flatter. This trend highlights an important feature of the impact of widths (σ/d_{sm}) of continuous PSDs, namely that cross-sectional uniformity of flux is better achieved throughout the riser for wider PSDs.

Finally, the other local measurement of interest includes the species segregation profiles in both the radial (Figure 13) and axial (Figure 14) directions. Analogous to the binary mixtures (Figures 7 and 8), each local mass % of coarse was normalized with respect to the system coarse for a more straightforward comparison. Similar to the binary mixtures (Figure 7), insignificant radial segregation is observed (Figure 13), which is again traced to the dilute nature of the flow and the small temperature gradients expected in such flows. In Figure 14 for the axial segregation, considering the identical ranges of the x-axes, interestingly, the extents of axial segregation (range of abscissa values) are similar for $\sigma/d_{sm} \geq 25\%$, while being least (most vertical profiles) for $\sigma/d_{sm} = 10\%$. Also, it is observed that the coarse composition generally decreases with height, which agrees with the binary work presented here (Figure 8) and previous work on binary and continuous PSDs.[19,30,31,45] Notably, as also

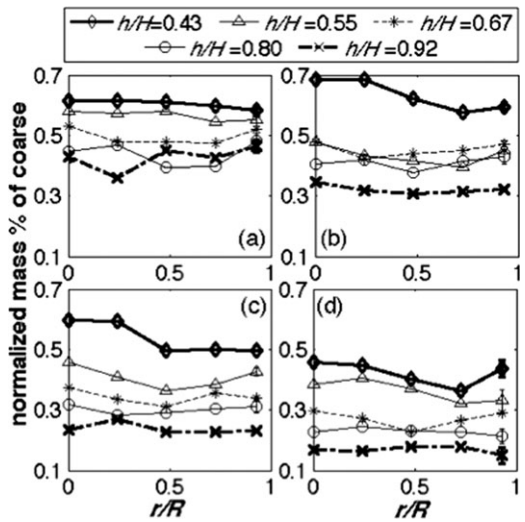

Figure 13. Radial segregation profiles of local mass % of coarse normalized with respect to the system mass % of coarse for continuous PSDs with σ/d_{sm} = (a) 10%, (b) 25%, (c) 40%, and (d) 65%.

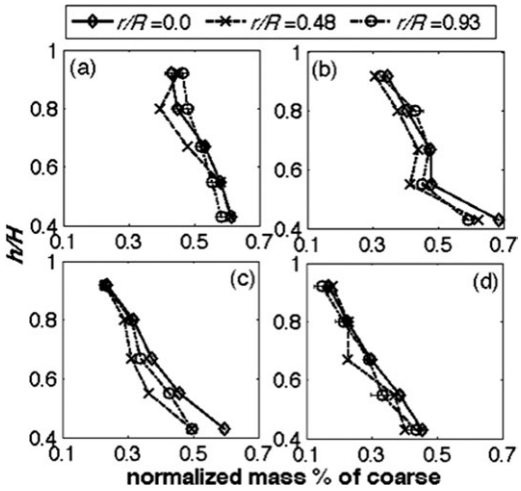

Figure 14. Axial segregation profiles of local mass % of coarse normalized with respect to the system mass % of coarse for continuous PSDs with σ/d_{sm} = (a) 10%, (b) 25%, (c) 40%, and (d) 65%.

pointed out by Chew et al.,[19] the axial segregation behavior at the wall represents an interesting qualitative difference between binary mixtures and continuous PSDs, in that a monotonic decrease of the more massive species with height is observed at all radial positions for the continuous PSDs (Figure 14), but the trend is nonmonotonic for the binary mixtures (Figure 8) near the wall.

Concluding Remarks

A comprehensive experimental suite with a focus on elutriation and species segregation phenomena of polydisperse Geldart Group B particles in a dilute CFB riser has been performed. Two categories of polydispersity were investigated: binary mixtures and continuous PSDs. The impact of polydispersity on various riser characteristics were investigated via varying (i) compositions of binary mixtures with two species differing in average particle diameter (d_{ave}) and material density (ρ_s), and (ii) widths of continuous PSDs while keeping the Sauter-mean diameter (d_{sm}) constant. Bulk measurements examined include elutriation flux (total and species and local measurements examined include mass flux and species segregation.

Before listing the observed differences between binary mixtures and continuous PSDs, it is worth noting that a key difference between the two types of polydispersity is that binary mixtures involves two discrete, but fixed, particle species (differing in size and/or density), while continuous PSDs involve a varying range of sizes (i.e., more species) as the distribution width increases. Notably, increasing the composition of fine particles ($U_t < U_s$) in binary mixtures is not equivalent to increasing the width (σ/d_{sm}) of continuous PSDs. Accordingly, three interesting observations on the qualitative differences in elutriation and species segregation characteristics between binary mixtures and continuous PSDs are highlighted: (i) whereas the increase of total elutriation flux is linked to an increase in mass % of fine for the binary mixtures, total elutriation flux and fine mass % show opposite trends for the continuous PSDs, (ii) while the elutriation flux of coarse particles ($U_t > U_s$) is nonmonotonic with respect to fine mass % for binary mixtures, coarse elutriation

flux is monotonic with fine mass % for continuous PSDs, and(iii) while the axial segregation of coarse particles at the wall do not decrease monotonically with riser height for binary mixtures, the same decrease is monotonic for continuous PSDs, both of which agree qualitatively with previous work.[19]

Three other interesting observations, which are common for both binary mixtures and continuous PSDs, deserve elaboration. First, why is the coarse species elutriated, even though the associated terminal velocity (U_t) is greater than the operating superficial gas velocity (U_s)? The physical picture for this counter-intuitive behavior is linked to the collisional transfer of momentum between the fine and coarse species. Specifically, the faster-moving fine ($U_t < U_s$) particles approach the coarse ($U_t > U_s$) particles and collide with them preferentially from the bottom, causing a net upward force on the coarse particle which hence enables the coarse to elutriate.[15] Second, radial mass flux profiles become flatter as either the composition of the binary mixture or the width of the continuous PSDs increases. This flattening effect is most apparent at the lowest axial position. Third, radial segregation is negligible for the dilute riser in this work, which is not surprising since species segregation is linked to granular temperature gradients,[4,33,46–51] and the radial granular temperature profile is expected to be relatively flat (i.e., small gradient) in dilute systems.[71]

The impact of polydispersity on the elutriation and species segregation phenomena reported in this work (together with a corollary work on cluster characteristics on the same system[77]) provide further insights into the dilute CFB riser behavior of both binary mixtures and continuous size distributions of Geldart Group B particles. Notably, the results reveal key qualitative differences between the behaviors of binary mixtures and continuous PSDs, as has been previously documented for bubbling fluidized beds[17,52–54,78] and a denser CFB riser (e.g. species segregation,[19] mass flux,[20] and clusters[79]). Such information is expected to be valuable not only in the validation of the numerous different kinetic-theory based models[4] for binary mixtures (for example, see Refs. [80] and [81]) but also for the application of such models (which are limited to a discrete number of species) to a continuous distribution.[82] Furthermore, it is expected that the application of such models will provide additional physical insight to the new behaviors reported here.

Acknowledgments

The authors gratefully acknowledge Particulate Solid Research Incorporated (PSRI) for the gifting of the extraction probe and useful discussions. The authors also thank the Department of Energy (DE-FC26-07NT43098) and National Science Foundation (CBET-0650893) for providing funding for this work.

Notation

CFB = circulating fluidized bed
d_{coarse} = average diameter of the coarse particles, μm
d_{fine} = average diameter of the fine particles, μm
d_{sm} = Sauter-mean particle diameter, μm
f_m = mass-based frequency distribution, μm^{-1}
f_n = number-based frequency distribution, μm^{-1}
G_r = local solid mass flux, kg/m^2/s
$G_{r,net}$ = net local solid mass flux, kg/m^2/s
G_s = overall solid mass flux, kg/m^2/s
$G_{r,net,norm}$ = net local solid mass flux normalized with overall solid mass flux (i.e., $\frac{G_{r,net}}{G_s}$)
h = height at which measurement was taken, m
H = total riser height, m
h/H = dimensionless height
m = solid loading
PSD = particle-size distribution
r = radius at which measurement was taken, m
R = total riser radius, m
r/R = dimensionless radius
U_s = superficial gas velocity, m/s
U_t = particle terminal velocity, m/s
ρ_g = gas density, kg/m^3
ρ_s = solid density, kg/m^3
σ = standard deviation of PSD, μm
σ/d_{sm} = width of PSD

Literature Cited

1. Sundaresan S. Some outstanding questions in handling of cohesionless particles. *Powder Technol*. 2001;115:2–7.
2. Muzzio FJ, Shinbrot T, Glasser BJ. Powder technology in the pharmaceutical industry: the need to catch up fast. *Powder Technology*. 2002;124:1–7.
3. Curtis JS, van Wachem B. Modeling particle-laden flows: A research outlook. *AIChE J*. 2004;50:2638–2645.
4. Hrenya CM. *Kinetic theory for granular materials: polydispersity*. In: Pannala S, Syamlal M, O'Brien T, editors. *Computational Gas-Solids Flows and Reacting Systems: Theory, Methods and Practice*. Hershey, PA: IGI Global, 2011;475:102–107.
5. Geldart D. Types of gas fluidization. *Powder Technol*. 1973;7: 285–292.
6. Leva M, Wen CY. *Elutriation*. In: Davidson JF, Harrison D, editors. *Fluidization*. New York, N.Y.: Academic Press, 1971:627–650.
7. Geldart D. *Elutriation*. In: Davidson JF, Clift R, Harrison D, editors. *Fluidization*. London: Academic Press, 1985:383–411.
8. Kunii D, Levenspiel O. *Fluidization Engineering*. 2nd ed. Newton, MA: Butterworth-Heinemann, 1991.
9. Fan LS, Zhu C. *Principles of Gas-Solid Flows*. New York, NY: Cambridge University Press, 1998.
10. Rhodes MJ. *Introduction to Particle Technology*. 1st ed. West Sussex, England: Wiley, 1998.
11. Tasirin SM, Geldart D. Entrainment of FCC from fluidized beds - a new correlation for the elutriation rate constants K-i infinity*. *Powder Technol*. 1998;95:240–247.
12. Baeyens J, Geldart D, Wu SY. Elutriation of fines from gas-fluidized beds of geldart A-type powders - effect of adding superfines. *Powder Technol*. 1992;71:71–80.
13. Ma XX, Honda Y, Nakagawa N, Kato K. Elutriation of fine powders from a fluidized bed of a binary particle-mixture. *J Chem Eng Jpn*. 1996;29:330–335.
14. Nakazato T, Kato K. Entrainment rates and elutriation rate constants of bed particles and group C fine powder in a fluidized bed and in a circulating fluidized bed. *J Chem Eng Jpn*. 2008;41:678–685.
15. Geldart D, Cullinan J, Georghiades S, Gilvray D, Pope DJ. Effect of fines on entrainment from gas-fluidized beds. *Trans Inst Chem Eng*. 1979;57:269–275.
16. Chew JW, Hays R, Findlay J, Knowlton TM, Karri SBR, Cocco RA, Hrenya CM. Reverse core-annular flow of Geldart group B particles in risers. *Powder Technol*. In press.
17. Chew JW, Wolz JR, Hrenya CM. Axial segregation in bubbling gas-fluidized beds with Gaussian and lognormal distributions of Geldart Group B particles. *AIChE J*. 2010;56:3049–3061.
18. Chew JW, Hrenya CM. Link between bubbling and segregation patterns in gas-fluidized beds with continuous size distributions. *AIChE J*. 2011;57:3003–3011.
19. Chew JW, Hays R, Findlay J, Knowlton TM, Karri SBR, Cocco RA, Hrenya CM. Species segregation of binary mixtures and continuous size distribution of Group B particles in riser flow. *Chem Eng Sci*. 2011;66:4595–4604.
20. Chew JW, Hays R, Findlay J, Knowlton TM, Karri SBR, Cocco RA, Hrenya CM. Impact of material property and operating conditions on mass flux profiles of monodisperse and binary mixtures Group B particles in the riser. *Powder Technol*. 2011;214:89–98.
21. Chew JW, Hays R, Findlay J, Knowlton TM, Karri SBR, Cocco RA, Hrenya CM. Cluster characteristics of Geldart Group B particles in a pilot-scale CFB riser. II. Polydisperse. *Chem Eng Sci*. 2012;68:82–93.
22. Hsiau SS, Hunt ML. Granular thermal diffusion in flows of binary-sized mixtures. *Acta Mech*. 1996;114:121–137.

23. Luding S, Strauss O, McNamara S. *Segregation of polydisperse granular media in the presence of a temperature gradient. IUTAM Symposium on Segregation in Granular Flows*. Boston: Kluwer Academic Publishers, 2000.
24. Xu H, Louge M, Reeves A. Solutions of the kinetic theory for bounded collisional granular flows. *Continuum Mech Thermodyn*. 2003;15:321–349.
25. Dahl SR, Hrenya CM. Size segregation in rapid, granular flows with continuous size distributions. *Phys Fluids*. 2004;16:1–13.
26. Galvin JE, Dahl SR, Hrenya CM. On the role of non-equipartition in the dynamics of rapidly flowing granular mixtures. *J Fluid Mech*. 2005;528:207–232.
27. Liu X, Metzger M, Glasser BJ. Couette flow with a bidisperse particle mixture. *Phys Fluids*. 2007;19:1–20.
28. Garzo V, Reyes FV. Segregation by thermal diffusion in granular shear flows. *J Stat Mech Theory Exp*. 2010;P07024.
29. Rowe PN, Nienow AW. Particle mixing and segregation in gas-fluidized beds - review. *Powder Technol*. 1976;15:141–147.
30. Nakagawa N, Bai DR, Shibuya E, Kinoshita H, Takarada T, Kato K. Segregation of particles in binary solids circulating fluidized-beds. *J Chem Eng Jpn*. 1994;27:194–198.
31. Hirschberg B, Werther J. Factors affecting solids segregation in circulating fluidized-bed riser. *AIChE J*. 1998;44:25–34.
32. Karri SBR, Knowlton TM. Flow direction and size segregation of annulus solids in a riser. In: Fan L-S, Knowlton TM, editors. *Fluidization IX*. Durango, CO: Engineering Foundation, 1998:189–196.
33. Lu HL, Gidaspow D. Hydrodynamics of binary fluidization in a riser: CFD simulation using two granular temperatures. *Chem Eng Sci*. 2003;58:3777–3792.
34. Dahl SR, Hrenya CM. Size segregation in gas-solid fluidized beds with continuous size distributions. *Chem Eng Sci*. 2005;60:6658–6673.
35. Cui HP, Grace JR. Fluidization of biomass particles: a review of experimental multiphase flow aspects. *Chem Eng Sci*. 2007;62:45–55.
36. Benyahia S. Verification and validation study of some polydisperse kinetic theories. *Chem Eng Sci*. 2008;63:5672–5680.
37. Liu X, Metzger M, Glasser BJ. Granular and gas-particle flows in a channel with a bidisperse particle mixture. *Chem Eng Sci*. 2008;63:5696–5713.
38. He Y, Deen NG, Annaland MVS, Kuipers JAM. Gas-solid turbulent flow in a circulating fluidized bed riser: numerical study of binary particle systems. *Ind Eng Chem Res*. 2009;48:8098–8108.
39. Nienow AW, Chiba T. *Fluidization of dissimilar materials*. In: Davidson JF, Clift R, Harrison D, editors. *Fluidization*. 2nd ed. Orlando, FL: Academic Press, 1985;733:367–382.
40. Lim KS, Zhu JX, Grace JR. Hydrodynamics of gas-solid fluidization. *Int J Multiphase Flow*. 1995;21:141–193.
41. Joseph GG, Leboreiro J, Hrenya CM, Stevens AR. Experimental segregation profiles in bubbling gas-fluidized beds. *AIChE J*. 2007;53:2804–2813.
42. Bai DR, Nakagawa N, Shibuya E, Kinoshita H, Kato K. Axial Distribution of solid holdups in binary solids circulating fluidized-beds. *J Chem Eng Jpn*. 1994;27:271–275.
43. Werther J, Hirschberg B. *Solids motion and mixing*. In: Grace JR, Avidan AA, Knowlton TM, editors. *Circulating Fluidized Beds*. London, UK: Blackie Academic and Professional, 1997;585:119–148.
44. Mathiesen V, Solberg T, Hjertager BH. An experimental and computational study of multiphase flow behavior in a circulating fluidized bed. *Int J Multiphase Flow*. 2000;26:387–419.
45. Das M, Meikap BC, Saha RK. Characteristics of axial and radial segregation of single and mixed particle system based on terminal settling velocity in the riser of a circulating fluidized bed. *Chem Eng J*. 2008;145:32–43.
46. Zhou HS, Flamant G, Gauthier D, Lu JD. Lagrangian approach for simulating the gas-particle flow structure in a circulating fluidized bed riser. *Int J Multiphase Flow*. 2002;28:1801–1821.
47. Lu HL, Liu WT, Bie RS, Yang LD, Gidaspow D. Kinetic theory of fluidized binary granular mixtures with unequal granular temperature. *Physica A*. 2000;284:265–276.
48. Lu HL, Gidaspow D, Manger E. Kinetic theory of fluidized binary granular mixtures. *Phys Rev E*. 2001;6406:061301.
49. Tartan M, Gidaspow D. Measurement of granular temperature and stresses in risers. *AIChE J*. 2004;50:1760–1775.
50. Biggs MJ, Glass D, Xie L, Zivkovic V, Buts A, Kounders MAC. Granular temperature in a gas fluidized bed. *Granular Matter*. 2008;10:63–73.
51. Songprawat S, Gidaspow D. Multiphase flow with unequal granular temperatures. *Chem Eng Sci*. 2010;65:1134–1143.
52. Hoffmann AC, Romp EJ. Segregation in a fluidized powder of a continuous size distribution. *Powder Technol*. 1991;66:119–126.
53. Gauthier D, Zerguerras S, Flamant G. Influence of the particle size distribution of powders on the velocities of minimum and complete fluidization. *Chem Eng J*. 1999;74:181–196.
54. Lin CL, Wey MY, You SD. The effect of particle size distribution on minimum fluidization velocity at high temperature. *Powder Technol*. 2002;126:297–301.
55. Hendrickson G. Electrostatics and gas phase fluidized bed polymerization reactor wall sheeting. *Chem Eng Sci*. 2006;61:1041–1064.
56. Guardiola J, Rojo V, Ramos G. Influence of particle size, fluidization velocity and relative humidity on fluidized bed electrostatics. *J Electrostat*. May 1996;37:1–20.
57. Ciborowski J, Wlodarski A. On electrostatic effects in fluidized beds. *Chem Eng Sci*. 1962;17:23–32.
58. Tardos G, Pfeffer R. A method to measure electrostatic charge on a granule in a fluidized-bed. *Chem Eng Commun*. 1980;4:665–671.
59. Osberg GL, Charlesworth DH. Elutriation in a fluidized bed. *Chem Eng Prog*. 1951;47:566–570.
60. Haider A, Levenspiel O. Drag coefficient and terminal velocity of spherical and nonspherical particles. *Powder Technol*. 1989;58:63–70.
61. Richardson JF, Zaki WN. The Sedimentation of a suspension of uniform spheres under conditions of viscous flow. *Chem Eng Sci*. 1954;3:65–73.
62. Dahl SR, Clelland R, Hrenya CM. The effects of continuous size distributions on the rapid flow of inelastic particles. *Phys Fluids*. 2002;14:1972–1984.
63. Rhodes MJ, Laussmann P, Villain F, Geldart D. *Measurement of radial and axial solids flux variations in the riser of a circulating fluidized bed*. In: Basu P, Large JF, editors. *Circulating Fluidized Bed Technology II*. Oxford: Pergamon Press, 1988:155–164.
64. Rhodes MJ, Laussmann P. Characterizing nonuniformities in gas-particle flow in the riser of a circulating fluidized-bed. *Powder Technol*. 1992;72:277–284.
65. Aguillon J, Shakourzadeh K, Guigon P. Comparative-study of non-isokinetic sampling probes for solids flux measurement in circulating fluidized-beds. *Powder Technol*. 1995;83:79–84.
66. Zhang WN, Johnsson F, Leckner B. Momentum probe and sampling probe for measurement of particle flow properties in CFB boilers. *Chem Eng Sci*. 1997;52:497–509.
67. Salvaterra A, Geldart D, Ocone R. Solid flux in a circulating fluidized bed riser. *Chem Eng Res Des*. 2005;83:24–29.
68. Zenz FA, Weil NA. A theoretical-empirical approach to the mechanism of particle entrainment from fluidized beds. *AIChE J*. 1958;4:472–479.
69. Berruti F, Chaouki J, Godfroy L, Pugsley TS, Patience GS. Hydrodynamics of circulating fluidized-bed risers - a review. *Can J Chem Eng*. 1995;73:579–602.
70. Tsuji Y, Morikawa Y, Shiomi H. Ldv measurements of an air solid 2-phase flow in a vertical pipe. *J Fluid Mech*. 1984;139:417–434.
71. Bolio EJ, Yasuna JA, Sinclair JL. Dilute turbulent gas-solid flow in risers with particle-particle interactions. *AIChE J*. 1995;41:1375–1388.
72. Herb B, Dou S, Tuzla K, Chen JC. Solid mass fluxes in circulating fluidized-beds. *Powder Technol*. 1992;70:197–205.
73. Wei F, Lu FB, Jin Y, Yu ZQ. Mass flux profiles in a high density circulating fluidized bed. *Powder Technol*. 1997;91:189–195.
74. Bader R, Findlay J, Knowlton TM. *Gas/solids flow patterns in a 30.5-cm-diameter circulating fluidized bed*. In: Basu P, Large JF, editors. *Circulating Fluidized Bed Technology II*. Oxford: Pergamon Press, 1988:123–137.
75. Marzocchella A, Arena U. Hydrodynamics of a circulating fluidized bed operated with different secondary air injection devices. *Powder Technol*. 1996;87:185–191.
76. Coronella CJ, Deng JX. A novel method for isokinetic measurement of particle flux within the riser of a circulating fluidized bed. *Powder Technol*. 1998;99:211–219.
77. Chew JW, Parker DM, Cocco RA, Hrenya CM. Cluster characteristics of binary mixtures and continuous size distributions of Group B particles in dilute riser flow. *Chem Eng J*. 2011;178:348–358.
78. Chew JW, Hrenya CM. Link between bubbling and segregation patterns in gas-fluidized beds with continuous size distributions. *AIChE J*. 2011;57:3003–3011.
79. Chew JW, Hays R, Findlay J, Knowlton TM, Karri SBR, Cocco RA, Hrenya CM. Cluster characteristics of Geldart Group B

particles in a pilot-scale CFB riser. I. Monodisperse. *Chem Eng Sci*. 2012;68:72–81.
80. Garzo V, Dufty JW, Hrenya CM. Enskog theory for polydisperse granular mixtures. I. Navier-Stokes order transport. *Phys Rev E*. 2007;76:031303.
81. Garzo V, Hrenya CM, Dufty JW. Enskog theory for polydisperse granular mixtures. II . Sonine polynomial approximation. *Phys Rev E*. 2007;76:031304.
82. Murray JA, Hrenya CM, Garzo V. Enskog theory for polydisperse granular mixtures. III. Comparison of dense and dilute transport coefficients and equations of state for a binary mixture. *Powder Technol*. 2012;22:24–36.

Manuscript received May 1, 2011, revision received Dec. 2, 2011, and final revision received Feb. 20, 2012.